A&A 369, 561–573 (2001)
DOI: 10.1051/0004-6361:20010194

Astronomy & Astrophysics

On the eclipsing nature of CPD − 59°2628⋆

L. M. Freyhammer[1,2], J. V. Clausen[3], T. Arentoft[1], and C. Sterken[1,⋆⋆]

[1] University of Brussels (VUB), Pleinlaan 2, 1050 Brussels, Belgium
[2] Royal Observatory of Belgium, Ringlaan 3, 1180 Brussels, Belgium
[3] Niels Bohr Institute for Astronomy, Physics and Geophysics; Astronomical Observatory, Juliane Maries Vej 30, 2100 Copenhagen Ø, Denmark

Received 9 August 2000 / Accepted 24 January 2001

Abstract. The spectroscopic binary CPD −59°2628 (Sp = O9.5 V) has been discovered to be a detached eclipsing binary, and we present an analysis based on new light curves, published spectroscopy and two new high-resolution spectra. *uvby* light curves from more than 2000 observations are analysed with the WINK and the Wilson–Devinney (WD) programs. Geometric distortions and photometric effects from the proximity of the components are included in the computations. The detached system has a close circular orbit of high inclination and high maximum projected velocities. We find a photometric period $P = 1\overset{\mathrm{d}}{.}47$ which is consistent with the spectroscopy–binary period by Solivella & Niemela (1999). We use this period to rematch the misidentified radial velocities from Levato et al. (1991) and apply them in an analysis using the method of Lehmann-Filhes. We find that CPD −59°2628 is a young system close to the ZAMS. Its distance is 2.6 ± 0.1 kpc and it has a systemic velocity of −19 km s^{-1}, confirming its membership in the cluster Trumpler 16 (radial velocity −23.5 km s^{-1}). The temperatures are 32 000 K for the hotter star (A) and 30 000 K for the cooler (B). We determine the absolute dimensions (solar units): $M_A = 14.0 \pm 2.0$, $R_A = 5.29 \pm 0.26$, $M_B = 11.7 \pm 1.8$ and $R_B = 4.38 \pm 0.22$. By adopting $E(b-y) = 0.306$, we get $M_{\mathrm{bol},A} = -6.3 \pm 0.1$, $M_{V,A} = -3.2 \pm 0.1$, $M_{\mathrm{bol},B} = -5.6 \pm 0.1$ and $M_{V,B} = -2.7 \pm 0.1$. Theoretical stellar models from Claret (1995), including convective–core overshooting and mass loss for a composition ($X = 0.70$, $Z = 0.02$), appear to fit the components at an age of ∼2 Myr.

Key words. stars: individual: CPD − 59°2628 – stars: binaries: spectroscopic – stars: binaries: eclipsing – stars: distances – stars: early-type

1. Introduction

In the framework of a long-term monitoring campaign of the Luminous Blue Variable η Carinae, we have obtained *uvby* time series data of a number of luminous stars located in the central part of the very young open cluster Trumpler 16. Photometry of Trumpler 16 members has been published by several authors but little, if anything, is known about the photometric variability of the brightest stars in the immediate neighbourhood of η Car. Kaltcheva & Georgiev (1993), for example, published Strömgren $uvby - \beta$ photometry of members of Trumpler 16, and derived colour excesses, distances, luminosities and temperatures. These authors put forward the idea that the brightest stars in Trumpler 16 do not belong to one physically related system, but are just a line of stars seen in projection. Such a geometry is possible because the region is the only place in our Galaxy where the line of sight is parallel to the ridge of our spiral arm. Our photometric analysis revealed that one of the central stars CPD −59°2628 (=Trumpler 16 1) – a known spectroscopic binary (Walborn 1982) – is also photometrically variable.

The spectroscopic-binary character of CPD −59°2628 was discovered by Walborn (1982), who classified the system as B0 with double lines. Almost a decade later Levato et al. (1991, hereafter LM) obtained 8 spectrograms of the system and derived a preliminary orbit characterised by $P = 5\overset{\mathrm{d}}{.}79$, $e = 0.08 \pm 0.05$, $K_A = 244 \pm 12$ km s^{-1}, $K_B = 287 \pm 12$ km s^{-1} and $V_\gamma = -20 \pm 6$ km s^{-1}. They found the systemic radial velocity to agree with the mean heliocentric radial velocity of the cluster (-23.5 ± 1.5 km s^{-1}). Recently, Solivella & Niemela (1999, hereafter SN) published preliminary orbital elements for CPD −59°2628 (see Table 5) based on some 40 spectra obtained over 8 years. They determine the period $P = 1\overset{\mathrm{d}}{.}469$ and the masses $M_A = 16 \pm 2\ M_\odot$ and $M_B = 14 \pm 2\ M_\odot$.

Send offprint requests to: L. M. Freyhammer,
e-mail: lfreyham@vub.ac.be

⋆ Based on observations obtained at the European Southern Observatory at La Silla, Chile (Applications 62H-0110, 62H-0110 and 64.L-0031) and the South African Astronomical Observatory, Sutherland, South Africa.

⋆⋆ Belgian Fund for Scientific Research (FWO).

Table 1. Catalogue data for CPD −59°2628 and comparison stars

		C_1	C_2	C_3
Trumpler 16	1	7	2	3
HD		303308		
CPD	−59°2628	−59°2623	−59°2632	−59°2627
α_{2000}	$10^h45^m08^s$	$10^h45^m06^s$	$10^h45^m11^s$	$10^h45^m07^s$
δ_{2000}	−59°40′50″	−59°40′06″	−59°41′12″	−59°41′57″
Sp. type	O9.5 V	O3 V	B1 V	O8.5 V
V	9.614	8.153	10.78	10.16
$(b-y)$	0.183	0.195		
m_1	−0.019	−0.020		
c_1	−0.048	−0.132		
β	2.607	2.596		

We have obtained complete *uvby* light curves of CPD −59°2628. Catalogue data (Kaltcheva & Georgiev 1993) for CPD −59°2628 and the comparison stars HD 303308 (C_1), CPD −59°2632 (C_2) and CPD −59°2627 (C_3) are given in Table 1.

2. Observations and data reduction

The photometric observations were obtained with three telescopes: the Dutch 0.9 m telescope at ESO, La Silla with the ESO #33 CCD (512 × 512 pixels, FOV 3.′5 × 3.′5), the 1.0 m telescope at SAAO, Sutherland, South Africa equipped with a SITE–4 CCD (1k × 1k pixels, FOV 6.′4 × 6.′4) and the Danish 1.5 m telescope, ESO, La Silla with DFOSC (2k × 2k LORAL–LESSER CCD, FOV 13.′7 × 13.′7). Finally two spectra were obtained in 2000 (JD 2 451 560 and 2 451 562) at the ESO 1.52 m, La Silla with FEROS (2k × 4k EEV CCD, thinned and backside–illuminated).

2.1. uvby photometry

We have obtained ∼2000 Strömgren-band CCD frames in 1997–1999 at the Dutch 0.9 m telescope in the Long–Term Photometry of Variables (LTPV) project (Sterken 1983, 1994). Integration times were optimised for η Car: about 4 s in 1997 (for y), and – due to the brightening of the central object (see Sterken et al. 1999) – gradually decreased to a mere 2 s in 1999. Typical integration times were: 15 s (u), 7 s (v), 4 s (b) and 2 s (y). During Jan–Mar 2000 the Danish 1.5 m telescope and the 1.0 m telescope, SAAO, were used for follow–up with additional 450 $uvby-\beta$ and H_α images, mainly to cover two eclipses. In order to observe η Car and keep exposure times longer than 1 s, the telescopes were brought slightly out of focus.

The *uvby* images were corrected for bias, flatfielded with sky-flats and reduced using aperture photometry based on the `DAOPHOT-II/IRAF` reduction package (Stetson 1987). Diaphragms were adjusted for the individual images with the Full–Width–Half–Maximum

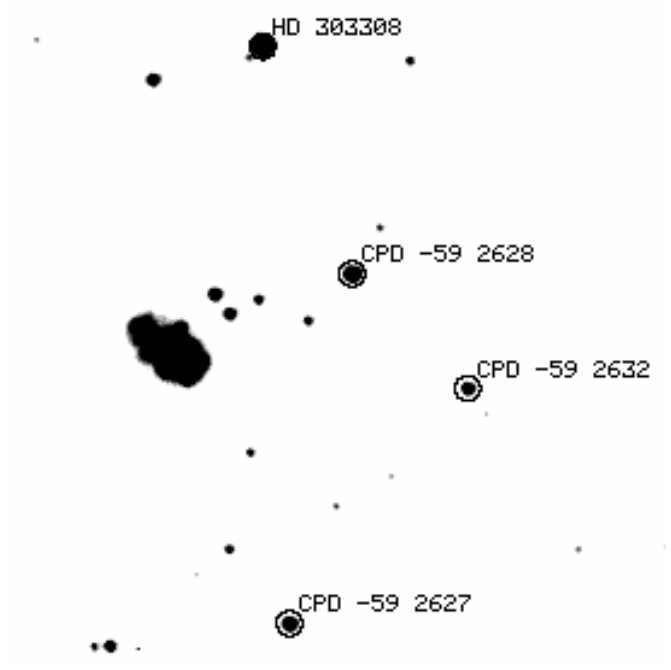

Fig. 1. 1.′9 by 1.′9 section of the field with CPD −59°2628, the comparison stars and η Car. N is up and E is right. HD 303308 was used for calibrating our photometry. 4.″7 diaphragms (= $4 \times FWHM$) are shown as circles. Note the faint neighbour SW of HD 303308

($FWHM$) measured in the images. Three diaphragm sizes were tested: 2×, 4×, and 6 × $FWHM$ diameter. The 4 × $FWHM$ diaphragm was selected based on the lower scatter in the comparison stars light curves. The median diaphragm size was 5.″1. The defocused 2000– observations introduced some scatter to the light curves due to minor effects from crowding and larger diaphragms. CPD −59°2628 and the comparison stars are displayed in Fig. 1 with a 4.″7–diaphragm overplotted. Background contribution to the stellar flux was determined as median flux inside a 6 × $FWHM$ wide and 2″ thick annulus, centered on the individual stars, and then removed.

Differential photometry was calculated for CPD −59°2628 using HD 303308 for comparison. HD 303308 has a close neighbour (Fig. 1) and is a spectroscopic binary (e.g. Massey & Johnson 1993), but with CPD −59°2632 and CPD −59°2627 as check stars it was found constant down to the theoretical (shot) noise $\sigma \sim 0.^m01$ of the light curves. Internal rms scatter in the CPD −59°2628 light curves is $0.^m007$ (u and b), $0.^m006$ (v) and $0.^m008$ (y). We removed the most deviating points by using a 1σ rejection level for the constant check star CPD −59°2627. We kept the data in the instrumental photometric system, but applied a zero–point correction to *uvby* photometry of HD 303308 from Kaltcheva & Georgiev (1993, their Table 1). The Dutch telescope filter set was renewed in 1997 and the majority of observations from this telescope were obtained using this new set. The same new filter set was used for all observations with the Danish telescope, while the SAAO filter set was

of different origin. We checked stability of these three filtersystems with photometry for CPD −59°2627 and out–of–eclipse data for CPD −59°2628. No systematic offsets were found in y, $(b-y)$, $(v-b)$ or $(u-v)$ down to $0\overset{\mathrm{m}}{.}01$ – the level of scatter in the time series.

2.2. Echelle spectroscopy

During two nights in 2000 at the ESO 1.52 m telescope, we obtained two high–resolution spectra (s9 and s10 in Table 4) of the binary. The FEROS instrument (Kaufer et al. 1999; Stahl et al. 1999) that was used is a fiber–fed Echelle spectrograph covering the range 3800–8600 Å with a resolving power of $R = 48\,000$. With two optical fibers, spectra were obtained simultaneously of CPD −59°2628 and a region of the sky 45″ west of CPD −59°2628. The spectra were obtained at the phases $\phi = 0\overset{\mathrm{p}}{.}765$ and $0\overset{\mathrm{p}}{.}405$ with 40 min integrations at the same airmass. As a spectroscopic template, a 300 s spectrum was obtained of HR 2928 (B2 III, $T_{\rm eff} = 26\,200$ K and $V = 5\overset{\mathrm{m}}{.}74$) within less than 10 percent higher airmass.

Flatfielding, background subtraction, order extraction, wavelength calibration and order merging were done with the MIDAS FEROS context, which allows very efficient on–line reduction. Skysubtraction was made by using sky spectra from the second optical fiber. High rotational– and orbital velocities of the components and interstellar (IS) bands made proper continuum windows non–existent over extended spectral regions. Therefore the continuum normalisation procedure was performed in two steps: i) a third–degree spline function was fitted to several points in proper continuum windows of the slow rotator HR 2928 ($v \sin i = 25$ km s^{-1}) and used to pre–normalise s9 and s10; ii) then rotationally broadened template spectra of O9.5 V – B0 V stars were used to select a few proper continuum windows in the pre–normalised s9 and s10, which were used to normalise the remaining large–scale continuum. The final continuum–normalised spectra cover the range from 3915–7500 Å and a section is displayed in Fig. 2. A "wobbling" pattern was left on a 2% level in the less line–dense region from 5000–6000 Å and the patterns coincide with the echelle–orders for every ∼140 Å. We did not attempt to correct for this since it was of the same order as the noise in the continuum.

The IS absorption lines CaII K, CaII H $\lambda\lambda$ 3934, 3968 and NaI $\lambda\lambda$ 5890, 5896 were used to check the wavelength calibration. The s9–s10 calibrations were in mutual agreement to within 2 km s^{-1} over the whole range, which indicates a stable spectrograph. Absolute wavelength calibration was verified with telluric oxygen and water vapour absorption lines from the line atlas by Catanzaro (1997). For the range 6880–7300 Å the calibrations agree within the measurement error of 3 km s^{-1}.

3. Spectroscopic analysis

Spectroscopic information on CPD −59°2628 in the literature is sparse. The only published line measurements are the radial velocities from LM based on 8 spectrograms at 43 Å mm^{-1} dispersion. The recent paper by SN gives preliminary orbital elements for the system, based on more than 70 radial velocities, but with considerable scatter in their measurements.

Table 2. Lines used from the s9–10 spectra of CPD −59°2628. † symbols indicate lines which were used in the profile synthesis analysis in Sect. 3.5. IS–lines are from Jenniskens & Désert (1994) and stellar lines are laboratory wavelengths

line (Å)	Identifier	note
4009.26	HeI	D
4026.19†	HeI	S, B
4101.74†	Hδ	
4120.98†	HeI	D, B, blend with Hδ
4199.87†	HeII	D, comp. *A* only
4340.47†	Hγ	
4387.93†	HeI	S, B, blend with Hγ
4471.48†	HeI	S, B
4541.59†	HeII	D, comp. *A* only
4647.42	CIII	S, B
4685.68†	HeII	S, B
4713.14	HeI	D, B
5875.63	HeII	D, B
3933.75	CaK	IS–lines
3968.41	CaH	–
5889.95	NaI	–
5895.92	NaI	–

D = diffuse; S = sharp; B = blend or multiplet.

We obtained the spectra s9–s10 included in Table 4. They cover the range from Hα to Hϵ and show broad and blended lines (Fig. 2). We used LM's radial velocity measurements to determine orbital parameters like the mass ratio $q = M_B/M_A$, checked with the new spectra, and through a non–LTE (NLTE) analysis of these, we determined temperatures and the luminosity ratio L_B/L_A. Lines used in the analysis of s9–s10 are given in Table 2.

3.1. Lines of the Carinae nebula

The two FEROS spectra show several prominent lines from nebula. The CaH, CaK and NaI absorption lines from Table 2 form line structures with more than four components in each. These components' radial velocities range from -105 to $+50 \pm 5$ km s^{-1} due to multiple ISM components in the line of sight. Levato & Malaroda (1982) found nebular emission in HeI λ4471, which can no longer be confirmed in s9–s10. Instead, strong double emission lines are seen inside Hα, Hβ and Hγ in the non–skysubtracted spectra. These lines are less prominent in the sky spectra and leave minor residuals in the skysubtracted spectra. In the 48 hrs elapsed between obtaining s9 and s10, the equivalent width (EW) of both double–lines in Hα and Hβ decreased 40% in the raw stellar spectra (no skysubtraction or continuum normalisation), while CaK for comparison remained constant within 1%. Variable β index of

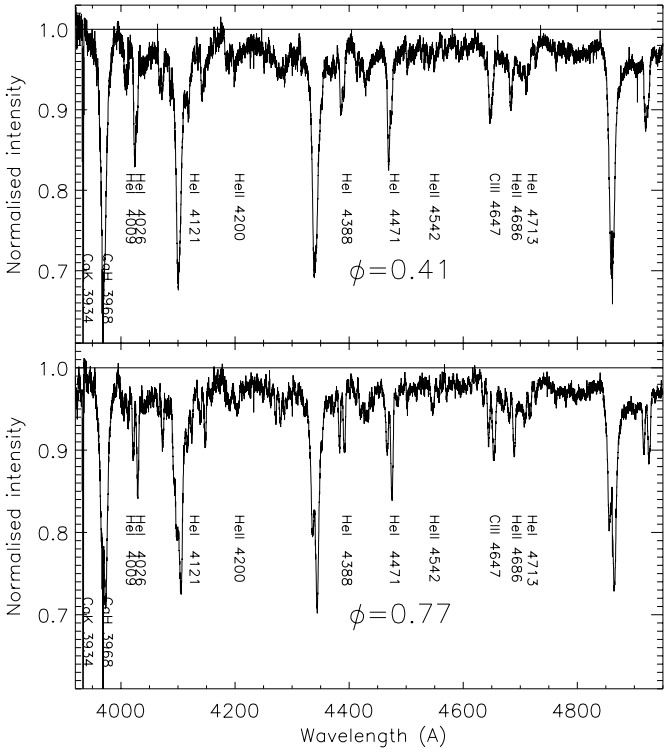

Fig. 2. A section of the two continuum normalised FEROS spectra, rebinned in bins of 0.15 Å. Note the IS CaH and CaK absorption lines, the DIB–structures at $\lambda\lambda$ 4428, 4750 and 4882 in Hβ and the residuals of the IS emission lines inside the Balmer lines. For other lines, such as HeI λ4471, any apparent central line emission is caused by line blending of the two stellar components (cf. Fig. 4)

CPD −59°2628 has been observed by E.H. Olsen (private communication) and can be due to such variablility in addition to radial velocity changes that shifts the Hβ–line in and out of the narrow β–passband. H$_\alpha$ and β–indices are thus not reliable in the case of CPD −59°2628. The double emission lines are separated by 46 km s^{-1} in both spectra. They are surely not related to CPD −59°2628 since they also appear in the sky spectra, but are probably emission lines from two different components of the η Car nebulosity complex moving with the projected velocities −34 and +11 km s^{-1}. Emission line measurements from the raw spectra are given in Table 3 where accuracy of the intensity is only an upper limit on the actual noise, because of the line variability. Sodium emission lines are present in all stellar and sky spectra of CPD −59°2628, but not in spectra of other targets from the same observing run. Their velocity shifts are 16 ± 2 km s^{-1} which corresponds to the heliocentric correction of 16 km s^{-1} applied in the wavelength calibration. The sodium lines might therefore be due to man–made light rather than the emission nebula.

3.2. Spectral types

Levato & Malaroda (1982) used double hydrogen and helium lines in their spectra of CPD −59°2628 to classify the binary as O9.5 V. The s9–s10 spectra show that

Table 3. Hα, Hβ and Hγ emission line parameters of CPD −59°2628 from the raw s9 and s10 spectra. V_V and V_R are the radial velocities of the violet and red components respectively, I is the intensity in the normalised spectra and $FWHM$ is the Full Width at Half Maximum of a Gaussian profile fit. Accuracy is estimated from the agreement between the two spectra for each parameter

	Hα	Hβ	Hγ	Accuracy
V_V (km s^{-1})	−35	−34	−34	1
I_V	0.39	0.09	0.03	0.07
$FWHM_V$ (km s^{-1})	30	34	26	3
V_R (km s^{-1})	12	12	10	1
I_R	0.74	0.19	0.06	0.10
$FWHM_R$ (km s^{-1})	26	25	24	2

temperatures are different for the two stellar components A and B since they have different line depths in hydrogen and helium, component A being more massive. Classification was attempted with the OB–star atlas from Walborn & Fitzpatrick (1990): HeII λ4200 and HeII λ4686 lines are only present from component A which place it earlier than B0.2 V and component B as later. The presence of the lines HeI λ4713, CIII λ4647 and HeII λ4686 from both components and their relative line strengths, place component A within O9.5 V — B0.2 V and component B not later than B0.5 V. Thus we classify CPD −59°2628 as O9.5 V+B0.3 V. Corresponding effective temperatures from FitzGerald (1970) and Popper (1980) are $30\,500 \pm 1800$ K (A) and $29\,500 \pm 1800$ K (B), or $31\,500 \pm 1500$ K and $28\,000 \pm 2000$ K from Böhm–Vitense (1981, Table 2). With the NLTE analysis in Sect. 3.5, we find final temperatures of $T_{\mathrm{eff},A} = 32\,000 \pm 500$ K and $T_{\mathrm{eff},B} = 30\,000 \pm 800$ K corresponding to the types O9.4 V and O9.9 V from Böhm–Vitense (1981).

3.3. Reanalysis of previously published radial velocities

During 9 consecutive nights LM obtained 8 spectrograms, each on a separate night around the same time ±1.6 hours. With such a small set of measurements and poor phase coverage, primary– and secondary line identifications become very difficult. By using 1–3 identified lines (their Table 1) they find the preliminary orbital parameters: period $P = 5\overset{\mathrm{d}}{.}79 \pm 0.06$, $K_A = 244 \pm 12$ km s^{-1} and $K_B = 287 \pm 12$ km s^{-1}. We used the photometric ephemeris (Sect. 4.1) to make a radial–velocity curve by using LM's K_A and K_B values, and fixed the radial velocities as $V_{r,A} = V_{r,B} = 0$ at the phase of the primary's minimum. Then all observed radial velocities were inserted and matched to the primary– and secondary components. As a check on this re–identification, we measured radial velocities in the new spectra s9–s10 from the HeI lines $\lambda\lambda$ 4009, 4026, 4388, 4471, 5876 and HeII λ4686. Line centers were determined from Gaussian profile fitting with the `IRAF noao.onedspec.splot` task. Component lines were rejected if they appeared blended when compared to a

Table 4. Primary/secondary radial velocities of CPD −59°2628 (km s^{-1}). n is number of lines measured and O–C is difference to computed velocities (Fig. 3). s1–s8 are from LM, Table 1, with swapped component lines for s2, s4 and s7. Spectra s9–s10 are new FEROS spectra, with rms scatter σ from all measured lines

Spec.	HJD	Star A			Star B			O–C	
ident.	2 400 000 +	Vel.	σ	n	Vel.	σ	n	A	B
s1	45778.77	−211		2	255		2	49	−15
s2	45779.76	125		2	−195		2	−19	20
s3	45780.79	99		2	−159		1	−11	14
s4	45781.69	−275		2	218		2	−21	−46
s5	45782.76	133		2	−217		2	43	−67
s6	45784.70	−283		3	327		3	−16	49
s7	45785.65	129		3	−189		3	−5	13
s8	45786.64	116		2	−163		2	32	−20
s9	51560.88	−147	11	4	191	15	5	11	24
s10	51562.88	268	8	4	−294	8	3	21	2

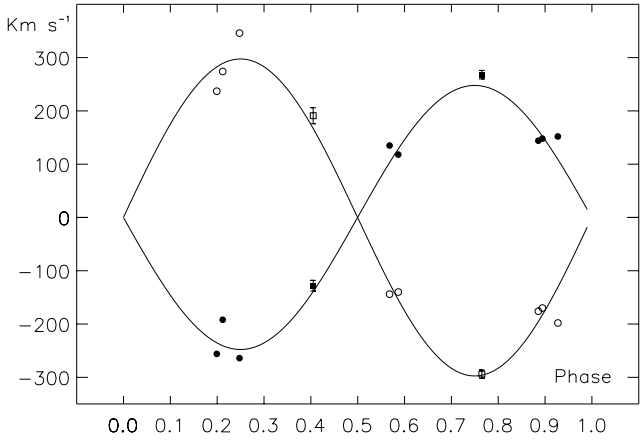

Fig. 3. Radial velocities for CPD −59°2628 and computed (SBOP, Table 5) orbits. Filled symbols are component A and empty symbols component B. Circles: Re–identified radial velocities from LM. Note that the radial velocities are grouped around the phases 0.2, 0.58 and 0.9 of the $1^{\rm d}.469332$ period. Squares: velocities from s9–s10 with rms error bars

broadened O9.5–template (NGC 2244 376). Table 4 gives the revised radial velocities from the spectra by LM (s1–s8) and from the recent spectra (s9–s10).

3.4. Mass ratio

The spectroscopic binary code SBOP (Etzel 1985) was applied to determine the adopted spectroscopic solution in Table 5, Col. 3 for fixed primary ephemeris and shown as a solid line in Fig. 3. SBOP uses the methods of Lehmann–Filhes (1894) and was applied to both components simultaneously.

The SBOP calculations were made with the following parameters fixed: the period P and epoch T_0 (calculated linearly from the one in Sect. 4.1), orbital eccentricity $e(=0)$ and ω the angle of periastron passage. Only radial velocity measurements from LM were used in the fit. Scaleable parameters were the maximum projected orbital velocities K_A and K_B and the systemic velocity V_γ. To test the revised radial velocity identifications, we calculated the elements with and without fixed ephemeris (T_0 for primary minimum). Both results are given in Table 5 and agree well. We adopted the solution with fixed ephemeris because of the more complete set of photometric data. In the last column (SN) of the table, the preliminary orbital elements by SN have been inserted for comparison and agree reasonably well with the SBOP solution. T_0 for SN has been calculated linearly from their ephemeris to the epoch of the SBOP calculations. The ephemeris of SN is given with T_0 for time of maximum radial velocity, which corresponds to 2 446 491.02 ± 0.01 at the time of primary minimum.

The SBOP solution yields the mass ratio $q = 0.83 \pm 0.08$ which is a reliable value when considering its small error, but the individual masses have large errors of about 12% due to the poor spectroscopic data and may be systematically wrong. Figure 3 shows the reanalysed (circles) and new (squares) radial velocities with the computed orbital solution. From the figure it appears that the reanalysed radial velocities are grouped around only three phases having a scatter of up to ±67 km s^{-1}. The reason for such large errors is probably line blending, as we also encountered in the two FEROS spectra (Sect. 3.3). LM used hydrogen and helium lines for their velocity measurements. Andersen et al. (1980) emphasise that the use of hydrogen and diffuse HeI lines in the case of young OB–stars can underestimate masses for similar luminosity ratio. Thus, errors in the determined masses can amount to 40% and 10% when using hydrogen and diffuse HeI lines, respectively.

In spite of large uncertainties in the computed solution from these errors, the computed orbits in Fig. 3 clearly agree with the radial velocities. The new measurements from s9–s10 solidifies the solution in two different phases. SN determine higher masses which lead to a higher mass ratio, and a slightly higher systemic velocity. The latter deviation cannot be explained alone by the given errors. As described in Sect. 5.1, the errors for the masses and maximum projected velocities of SN are not consistent, and at least some of their error estimates may be optimistic.

3.5. Rotation rates and luminosity ratios

The preliminary analysis of the photometry with WINK and WD (Sect. 4.3) shows that the light curves alone do not constrain the ratio of radii $k = r_B/r_A$ well enough. We therefore need to use s9 and s10 in order to determine L_B/L_A and thereby k. The high-resolution spectra also allow determination of the effective temperatures of the components. Only the ratio between the effective temperatures (surface flux ratio) can be obtained from the light curve analyses.

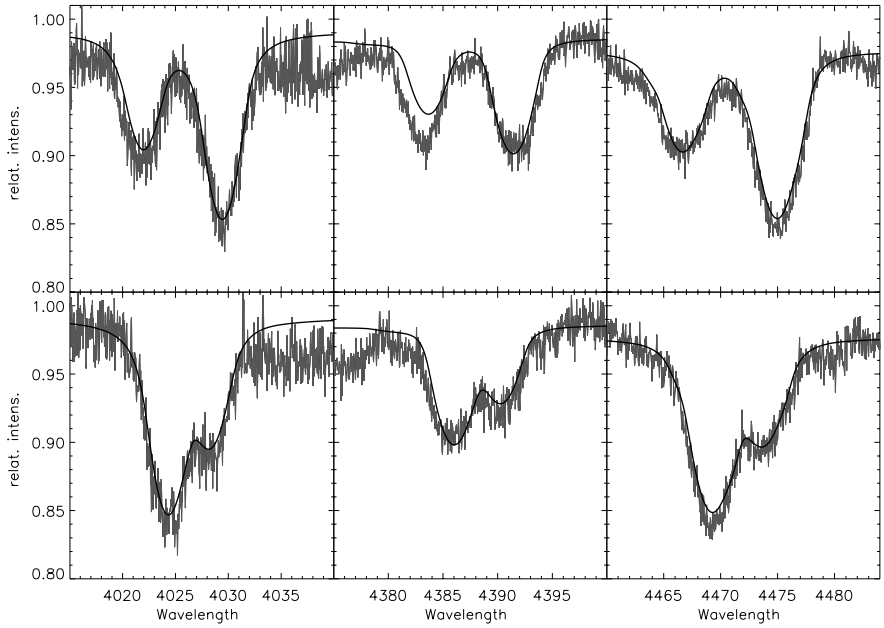

Fig. 4. Lines from the non–LTE analysis. Left to right: HeI λλ4026, 4388 and 4471. Lower and upper panels are s9 and s10, respectively. Best model overplotted as thick line

Table 5. SBOP spectroscopic orbital solutions for CPD −59°2628. No weights used. Fixed values: P, $e = 0$ and $\omega = 180°$. Epoch T_0 is for the time of primary minimum. For comparison the solution by SN is given in the last column

Elements	T_0, free	T_0, fixed	SN
T_0(HJD-2 400 000)	50452.414 ±12	50452.408	50452.44 ±1
Period (days)	$1\overset{\mathrm{d}}{.}469332$	$1\overset{\mathrm{d}}{.}469332$	$1\overset{\mathrm{d}}{.}46937$ ±1
V_γ (km s^{-1})	-18.9 ± 9.3	-19.0 ± 9.0	-5 ± 4
K_A (km s^{-1})	248 ± 18	248 ± 17.4	268 ± 8
K_B (km s^{-1})	298 ± 18	298 ± 17.4	314 ± 8
$a_A \sin i$ ($R_\odot$)	7.19 ± 0.52	7.19 ± 0.50	8 ± 0.2
$a_B \sin i$ ($R_\odot$)	8.64 ± 0.52	6.64 ± 0.50	9 ± 0.2
$M_A \sin^3 i$ ($M_\odot$)	13.5 ± 1.5	13.5 ± 1.4	16 ± 2
$M_B \sin^3 i$ ($M_\odot$)	11.2 ± 1.3	11.2 ± 1.3	14 ± 2
M_B/M_A	0.83±0.08	0.83 ± 0.08	0.88
σ(1 obs.) (km s^{-1})	36.9	35.9	

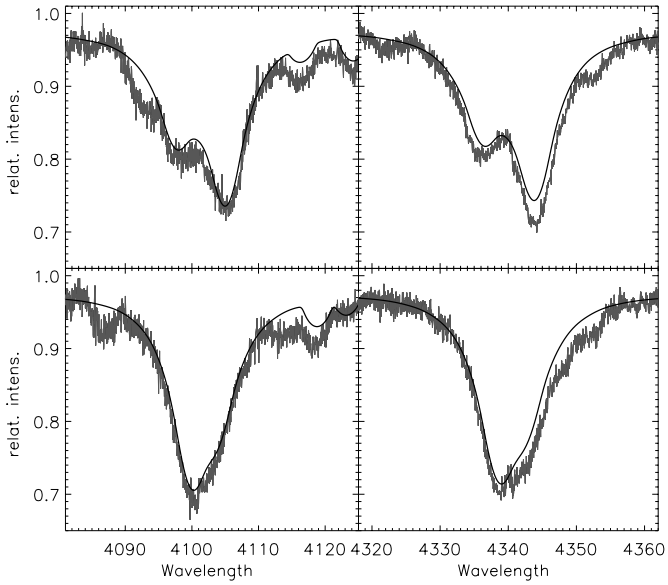

Fig. 5. Like Fig. 4 but for Hδ with HeI λ4121 (left) and Hγ (right). Note inconsistencies in the wings due to blended lines and in the depth of the lines. Also note the IS emission line residuals, strongest in Hγ

The spectral lines in s9–s10 (Fig. 2) are broad with typical line depths of 5–10%, Balmer lines excepted. Blends are common and Diffuse Interstellar Bands (DIB) are significant at several places in the spectra: i.e. the continuum in the region λ4750–λ4960 is suppressed by ∼2% as compared to a broadened template spectrum of the closer star NGC 2244 376 (∼1.4 kpc distance, e.g. Hensberge et al. 2000), due to a structure of wide DIB's (Tuairisg et al. 2000). The spectral classification in Sect. 3.1 indicated high effective temperatures $T_{\mathrm{eff},A}$ and $T_{\mathrm{eff},B}$ of about 30 000 K and significant temperature differences. For that reason is it not straightforward to associate EW–ratios with luminosity ratio (Vaz et al. 1997) and we are therefore indebted to H. Hensberge who very kindly provided NLTE model lines, crucial for the spectral analysis of CPD −59°2628.

EW measurements are very sensitive to errors from continuum displacements and line blending, so we chose to determine temperatures and luminosity ratio by comparing the spectra with synthesised line profiles, while checking the local continuum with a broadened template spectrum of the slow rotator ($v \sin i = 35$ km s^{-1}) NGC 2244 376 ($V = 9.70$, O9 V, Ogura & Ishida 1981 and references therein). Synthetic spectral lines used in the NLTE analysis are based on LTE line–blanketed continuum models of Kurucz (1992) for solar abundances and depth dependent NLTE line formation computations performed with the DETAIL and SURFACE software codes

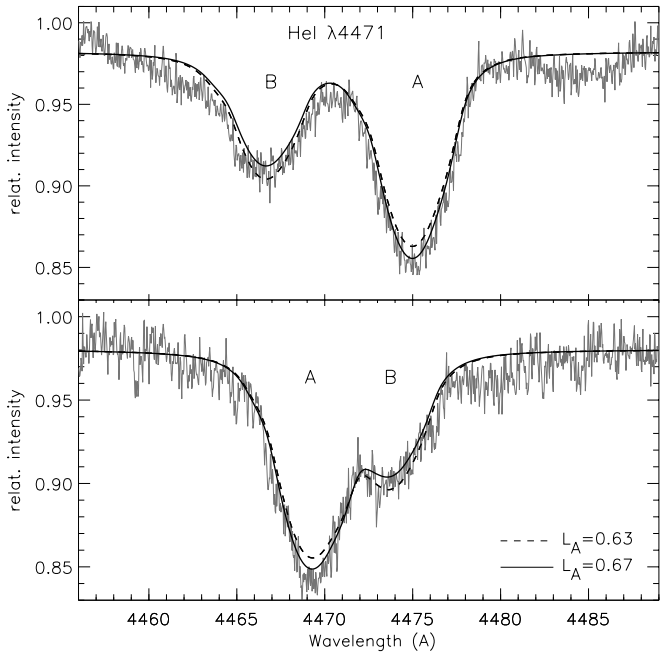

Fig. 6. Like Fig. 4 for HeI λ4471, but with two non–LTE models for different luminosity ratio $L_A(=1-L_B)$. Disagreements between models and the spectra are due to line–blending, which was confirmed by comparison with a broadened spectrum of a slow rotator of same type

(Giddings 1981; Butler 1994). References for computations and models can be found in Vrancken et al. (1997). For rotational broadening the line profiles were convolved with the rotation profile from Gray (1976).

Seven spectral lines were selected as listed in Table 2 and synthesised as NLTE model lines. For Hγ and Hδ the models also included the close HeI lines $\lambda\lambda$ 4388, 4121. The seven lines were selected after criteria for sharpness, blending conditions and sensitivity to physical parameters of the stars. Non–singlet lines, marked as "blended lines" in the table, have been reproduced with all additional components. All lines were reproduced for different temperatures, surface gravities, luminosity ratios and rotational– and radial velocities. Synthetic lines for both stars were then combined and fitted by eye to s9 and s10. Starting values for the parameters were taken from the orbital solution in Table 5 and preliminary WINK solutions for the photometry, and then optimised sequentially one by one. As predicted by NLTE-calculations, HI and HeII lines are respectively more gravity– and temperature sensitive and thus we added more weight to these lines when fixing such parameters. First guesses of rotational velocities $v_A \sin i$, $v_B \sin i$, were obtained with the $v \sin i$ — linewidth table from Slettebak (1975). HeI λ4471 linewidths in s9 and s10 are: $FWHM_A = 4.8 \pm 0.1$ and $FWHM_B = 4.3 \pm 0.2$ Å, which by interpolation in the table for five O9 III—B0.3 IV stars yield $v_A \sin i = 173 \pm 9$ km s^{-1} and $v_B \sin i = 150 \pm 8$ km s^{-1}. The adopted NLTE-model is characterised by the following parameters:

$$V_{r,A}(\mathrm{s9}) = -140 \pm 10\,\mathrm{km\,s^{-1}} \quad V_{r,B}(\mathrm{s9}) = 175 \pm 10\,\mathrm{km\,s^{-1}}$$
$$V_{r,A}(\mathrm{s10}) = 250 \pm 10\,\mathrm{km\,s^{-1}} \quad V_{r,B}(\mathrm{s10}) = -310 \pm 10\,\mathrm{km\,s^{-1}}$$
$$T_{\mathrm{eff},A} = 32\,000 \pm 500\ \mathrm{K} \quad T_{\mathrm{eff},B} = 30\,000 \pm 800\ \mathrm{K}$$
$$v_A \sin i = 170 \pm 10\,\mathrm{km\,s^{-1}} \quad v_B \sin i = 150 \pm 10\,\mathrm{km\,s^{-1}}$$
$$L_A = 0.65 \pm 0.02$$

where $V_{r,A}$ and $V_{r,B}$ are radial velocities. Errors are estimated by varying single parameters individually, such as in Fig. 6 where the effect of different values of L_A is shown for HeI λ4471. Synchronous rotation for the two components requires $v_A \sin i > v_B \sin i$ since star A is larger than B, which is true for the found parameters above. Because of this, and for simplicity, synchronous rotation is assumed for the two components. Figures 4 and 5 show selected HeI and HI lines with the final model overplotted. As reproduced by the models, HeII $\lambda\lambda$ 4200, 4542 are only significant in the primary component's spectrum. In general the fit to the HeII lines are worse than for the HeI lines, because they are either weaker or the local continuum is suppressed by several other lines (see Fig. 2). The model lines do otherwise fit the spectrum lines well for both s9 and s10 with minor inconsistencies due to blending. Examples are HeI λ4388, where line blending with lines from higher wavelength occurs, and Hδ where the continuum is not well defined. As found by Hensberge et al. (2000), the depth of the Balmer lines is not reproduced well by the models. The radial velocities deviate from those of Table 4, but are within the common scatter, and demonstrate the difficulties of fitting line blends with simple Gauss profiles. From the relative luminosity L_A, we get $L_B/L_A(\lambda) = 0.54 \pm 0.05$ for the analysed wavelength range 4000–5000 Å.

4. Photometric analysis

Figure 7 shows the complete y light curve and binned $(b-y)$, $(v-b)$, $(u-v)$ colour curves with theoretical light curves (Table 8). Phase $0\overset{\mathrm{p}}{.}0$ in the diagram was fixed to the primary minimum (Sect. 4.1). The eclipses are relatively broad, of equal width and with only $0\overset{\mathrm{m}}{.}1$ difference in depth. During primary eclipse a colour change towards red is visible in $(u-v)$, and during secondary eclipse a small shift towards the blue is seen in $(v-b)$. This indicates well–separated, large stars of similar spectral type. Variations of $0\overset{\mathrm{m}}{.}05$ outside the eclipses indicate the presence of reflection effects and/or deformation of the components. The secondary minimum occurs at phase 0.5 as confirmed by our only observed secondary eclipse (see Table 6), which together with equally broad eclipses and short period indicate a circular orbit.

4.1. Ephemeris and period analysis

The *uvby* photometry contains four primary and one secondary minima observed during 1997–2000 as listed in Table 6. Minimum No. 5 was observed extensively in several colours and solidifies the final ephemeris below. Times

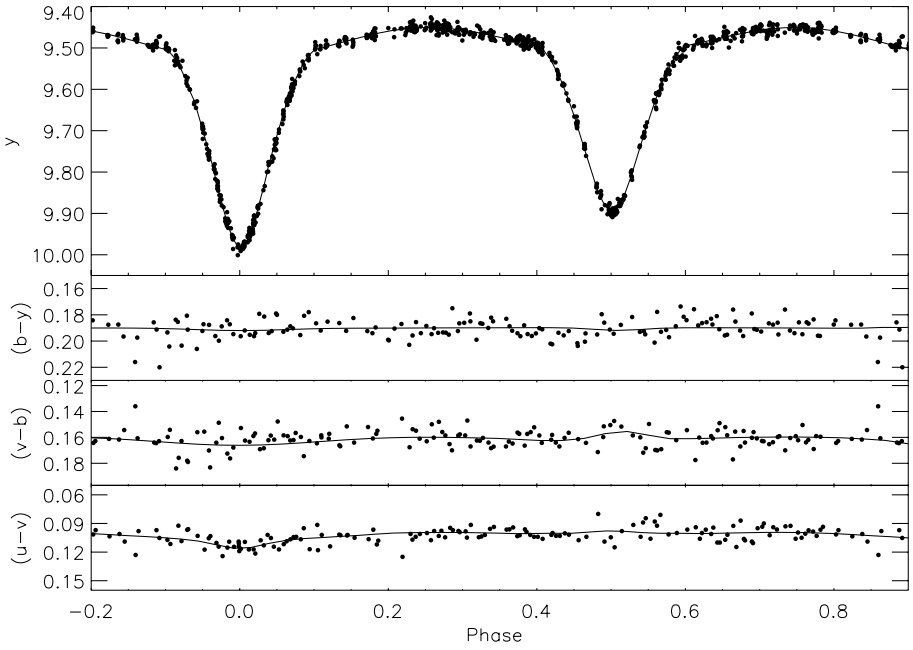

Fig. 7. y light curve and binned (bins of $0\overset{p}{.}005$) $b-y$, $v-b$ and $u-v$ colour curves for CPD −59°2628. The four theoretical curves represent the solution in Table 8

Table 6. Times of minimum

No.	HJD 2 400 000 +	σ	O–C	Type	Method
1	50456.819	$0\overset{d}{.}002$	$+0\overset{d}{.}0026$	pri	polyn.
2	50481.791	$0\overset{d}{.}001$	$-0\overset{d}{.}0040$	pri	K&VW
3	50487.674	$0\overset{d}{.}001$	$+0\overset{d}{.}0016$	pri	K&VW
4	51565.428	$0\overset{d}{.}001$	$+0\overset{d}{.}0009$	sec	polyn.
5	51592.6091	$0\overset{d}{.}0005$	$-0\overset{d}{.}00065$	pri	K&VW

of minimum light were calculated by means of the Kwee & van Woerden (1956) method and second order polynomial least–square fit and are given in Table 6. Deviation from the linear ephemeris, O–C does not indicate any systematic variation in the residuals even though it exceeds the scatter of the fitted minima. We find the following linear primary ephemeris:

$$\begin{array}{c}\text{Min } A\text{: } 2\ 450\ 456.8164 + 1\overset{d}{.}4693316 \cdot E \\ \qquad\qquad\quad \pm 15 \qquad\quad \pm 33\end{array}$$

without using weights. Minimum No. 4 was included since we have assumed $e = 0$, and did not alter the ephemeris significantly. We select the epoch (T_0) of the ephemeris as the time of the primary star's minimum, i.e. when it is eclipsed by the secondary component. The spectroscopic period from SN is less precise than the one above, but the small difference is significant. The linearly calculated ephemeris above has $0\overset{p}{.}05$ phase offset to the ephemeris by SN.

4.2. Binary model input parameters

Preliminary analyses were performed with the `WINK` (e.g. Wood 1971) binary code (references for this version: Vaz & Nordlund 1985; Vaz 1986; Nordlund & Vaz 1990) and the final solutions with the more sophisticated `WD` (Wilson & Devinney 1971; Wilson 1993) code (additional reference for this version: Vaz et al. 1995).

From the photometry of Kaltcheva & Georgiev (1993) and calibrations of Crawford (1975), we got the $uvby-\beta$ standard indices in Table 1, reddening of $E(b-y) = 0.306$, and absorption in the visible of $A_V = 1\overset{m}{.}314$. The unreddened $(b-y)_0 = 0\overset{m}{.}190$ index, then corresponds to a mean system temperature of about 30 000 K while the spectra gave temperatures about 1000 K higher. We take as a starting value the effective temperature 32 000 K for component A. Atmosphere models from Kurucz (1979) were adopted for better agreement with the spectroscopy than with plain black body models. $T_{\mathrm{eff},A}$ was fixed and $T_{\mathrm{eff},B}$ left as a free parameter in the computations.

Reflection albedos and gravity darkening exponents were fixed at 1.0. We adopted the linear limb darkening coefficients (assuming $T_{\mathrm{eff},B} = 30\,000$ K) from Diaz-Cordoves et al. (1995):

$u_u = 0.35$; $u_v = 0.34$; $u_b = 0.31$; $u_y = 0.29$ (A),
$u_u = 0.36$; $u_v = 0.35$; $u_b = 0.33$; $u_y = 0.29$ (B),

and the bolometric limb darkening coefficients: 0.54 (A) and 0.56 (B) from van Hamme (1993). Circular orbit, synchronous rotation of the components and no third light were assumed.

The spectroscopic estimate of L_B/L_A yields $k \sim 0.82$, based on the theoretical flux ratio of $F_B/F_A = 0.80$ from NLTE atmosphere models for temperatures of 30 000 and 27 000 K. Therefore $k = 0.8$ was used as starting value, which is also a ratio found for similar binaries such as the V3903 Sgr (O7 V+O9 V, Vaz et al. 1997) and V578 Mon (early–B, Hensberge et al. 2000).

Table 7. Initial solution for CPD −59°2628, obtained with the WINK model, the *uvby* light curves and the mean spectroscopic elements. $T_{\rm eff,A} = 32\,000$ K and $k = 0.825$ (fixed). Phase shift $d\phi$ is given in phase units

	y	b	v	u	Mean
i	80.°47	80.°36	80.°12	80.°09	80.°26
	±6	±7	±8	±10	±18
$T_{\rm eff,B}$ (K)	29 008	28 908	28 766	28 911	28 898
	±66	±86	±101	±112	±100
r_A	0.3255	0.3255	0.3274	0.3302	0.3272
	±6	±6	±7	±8	±22
r_B	0.2685	0.2685	0.2701	0.2724	
$r_A + r_B$	0.5940	0.5940	0.5975	0.6026	
L_B/L_A	0.556	0.5528	0.5408	0.5161	
$d\phi$	0.0014	0.0014	0.0013	0.0015	0.0014
	±1	±1	±2	±2	±2
σ (mmag)	9	8	8	9	

4.3. Determination of the photometric elements

The preliminary analysis of our photometric data was performed using the WINK binary model to explore the solution space. This model, which is based on three axial ellipsoids and includes a fairly realistic model for reflection effects, is well suited for analysis of detached systems with moderately large (about 0.25) relative radii. Furthermore, it is efficient for calculation of large grids of test runs. First, the model was applied to the y light curve which has most observations and when a plausible solution was found, we added the *bvu* data to the analysis.

The stellar parameters to be solved for are: the orbital inclination i, temperature T_B of component B, relative radius r_A of the primary, luminosity ratio L_B/L_A and the phase shift $d\phi$. Solutions with different ratio of stellar radii $k(= r_B/r_A)$ were tested and we found k to be poorly constrained by the photometry, which gave acceptable solutions for $k = 0.8{-}1.0$. WD (see below) showed the same large range of acceptable k, but with $T_{\rm eff,A}$ and $T_{\rm eff,B}$ from the spectra it did actually converge to a solution with the ratio $k = 0.83$. The corresponding luminosity ratio was consistent with the one from the spectra, and because the solution had good agreement for all four bands, we found it reliable and fixed k to 0.83 in WINK.

The corresponding WINK solution is given in Table 7. It shows that CPD −59°2628 is a close binary system of similar components, which are massive but well–detached and well inside their Roche lobes ($r_{\rm Roche} \sim 0.38$). The system has a high inclination of $i = 80.°3$ and components with high similar temperatures. Good agreement between the *uvby*–bands is seen, i.e. for the sum of the stellar radii. Note that the radii r_A, r_B are relative, given in units of the orbital semi–major axis.

The WD binary model, which is based on Roche configurations, was used for the final computations because the close and massive nature of the system indicates that secondary effects, like reflected light and stellar deformations, are significant. Mode 2 was assumed throughout the analysis, i.e. a detached configuration. The following procedure was used: individual light curve solutions are made, which as opposed to a combined light curve solution, give high sensitivity to third light and provide independent errors for the final photometric elements; then we fix the stellar dimensions to the solutions mean values and calculate individual solutions in order to determine luminosity ratios in *uvby*.

A series of solutions was computed to explore the influence and stability of the adjustable parameters. The solutions show good mutual agreement colour by colour, which is an independent check of their consistency. Introduction of atmosphere model tables of Kurucz (1979) was clearly a better approximation than blackbody radiation to produce temperatures matching the spectroscopy. $T_{\rm eff,B}$ was thus increased by 1000 K and a small but significant change is seen in the geometry, the latter probably being due to high deformation of the stars. In particular r_A

Table 8. Wilson-Devinney binary model solutions for the four light curves and mean photometric elements for CPD −59°2628. Circular orbit and $q = 0.83$ were assumed. $T_{\rm eff,A} = 32\,000$ K (fixed). $l_A(\phi_{0.25})$, $l_B(\phi_{0.25})$ are light contributions at phase 0.p25

	y	b	v	u	Mean
i	80.°70	80.°52	80.°38	81.°70	80.°58
	± 5	± 6	± 5	± 10	± 16
$T_{\rm eff,B}$ (K)	29 058	29 157	29 077	29 133	29106
	± 39	± 51	± 60	± 60	± 46
Ω_A	3.9346	3.9542	3.9342	3.9150	3.9346
	± 53	± 83	± 58	± 68	± 158
Ω_B	4.1945	4.1597	4.1569	4.2021	4.1783
	± 76	± 131	± 83	± 122	± 233
L_A	5.140	5.141	5.179	5.379	
	± 15	± 29	± 21	± 26	
L_B	2.866	2.986	2.923	2.764	
L_B/L_A	0.558	0.581	0.564	0.514	
$l_A(\phi_{0.25})$	0.4156	0.4156	0.4190	0.4359	
$l_B(\phi_{0.25})$	0.2334	0.2435	0.2388	0.2270	
$l_B/l_A(\phi_{0.25})$	0.562	0.586	0.570	0.521	
$d\phi$	0.0012	0.0014	0.0010	0.0013	0.0012
	± 1	± 1	± 1	± 1	± 2
$r_{A,\rm pole}$	0.3181	0.3162	0.3181	0.3200	0.3181
$r_{A,\rm point}$	0.3533	0.3502	0.3534	0.3565	0.3533
$r_{A,\rm side}$	0.3281	0.3260	0.3282	0.3303	0.3281
$r_{A,\rm back}$	0.3418	0.3393	0.3419	0.3444	0.3418
$< r_A >$	0.3298	0.3276	0.3298	0.3320	0.3298
					± 18
$r_{B,\rm pole}$	0.2641	0.2670	0.2672	0.2635	0.2655
$r_{B,\rm point}$	0.2839	0.2880	0.2883	0.2831	0.2858
$r_{B,\rm side}$	0.2697	0.2729	0.2731	0.2690	0.2712
$r_{B,\rm back}$	0.2787	0.2824	0.2827	0.2780	0.2804
$< r_B >$	0.2711	0.2744	0.2746	0.2704	0.2726
					± 22
$< k >$	0.822	0.838	0.833	0.814	0.827
					± 11
σ (mag)	0.0088	0.0073	0.0072	0.0080	
# obs	951	582	441	339	

Table 9. Wilson-Devinney binary model solution for fixed mean geometry from Table 8 for CPD −59°2628. $q = 0.83$ assumed

	y	b	v	u
$T_{\rm eff,B}$ (K)	29 056	29 106	29 149	29 155
	± 38	± 47	± 46	± 46
L_A	5.141	5.149	5.169	5.372
	± 5	± 6	± 6	± 8
L_B	2.898	2.903	2.891	2.850
L_B/L_A	0.564	0.564	0.559	0.531
$l_A(\phi_{0.25})$	0.4156	0.4164	0.4182	0.4349
$l_B(\phi_{0.25})$	0.2362	0.2367	0.2369	0.2343
$l_B/l_A(\phi_{0.25})$	0.568	0.568	0.566	0.539
σ (mag)	0.0088	0.0074	0.0073	0.0080

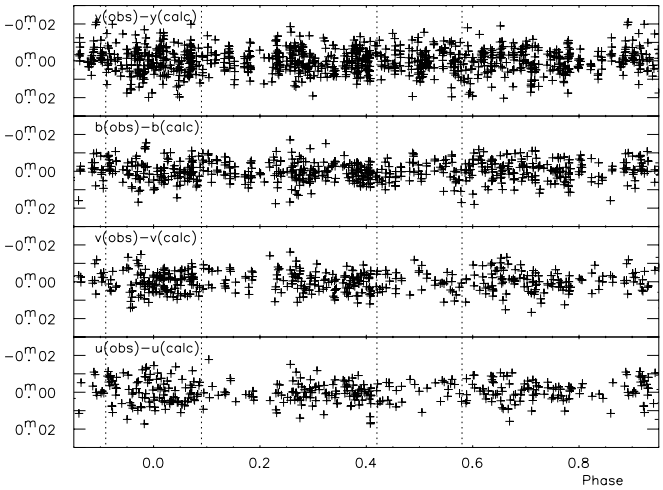

Fig. 8. Residuals of the *uvby* observations from the theoretical light curves (Table 8). Dotted lines delimit the start and end of both eclipses. From top to bottom: O–C for y, b, v and u

was affected and decreased about one percent. However, the large uncertainty on the mass ratio q of 0.08 contributes significantly to the uncertainty of the solutions. Furthermore, different bands give differences of about 3% in k, which is not surprising since k for partially eclipsing components of nearly identical dimensions is generally not well constrained by light curves alone. The acceptable range of k is 0.7–1.2 while the luminosity ratio changes correspondingly 0.4–1.2, thus we cannot consider WD solutions reliable unless confirmed independently by spectroscopy.

Starting values were taken from the *uvby*–set of WINK-solutions in Table 7, Col. 6, and the mass ratio q was taken from the SBOP solution (Table 5). The following parameters are adjusted: temperature of the secondary component $T_{\rm eff,B}$, stellar potentials Ω_A and Ω_B, luminosity of the primary L_A and phase shift $d\phi$. Fixed values are: $T_{\rm eff,A}$ and mass ratio $q = 0.83$.

The corresponding *uvby*–set of solutions is given in Table 8. $L_{A,B}$ are 4π steradian luminosities. From the axes of the relative stellar radii, it is seen that the stars are deformed significantly, amounting to 10% and 7% difference of the A and B component axes, respectively. The luminosity ratio agrees well with the spectroscopic result from Sect. 3.5. Column 6 in the table gives the mean elements which are adopted as the final elements. Figure 8 shows the residuals for this solution. The largest residuals are seen during primary eclipse, but no systematic features are seen. Mean elements for the two components are given in Table 10.

In order to estimate the errors for the stellar radii, WD–solutions were computed for different values of T_A, k, L_B/L_A (by changing the potentials) and q within their allowed errors from Table 8: adjusting L_B/L_A (by changing Ω_B) inside its 1σ (=0.055) error range results in 4σ changes in k and the individual stellar radii; 1σ (= 0.08) adjustments of q, with L_B/L_A fixed to 0.556 (otherwise L_B/L_A exceeds its spectroscopic value), cause only minor changes in k and the radii inside their allowed 1σ errors; finally, changing T_A 1000 K does not affect k or the radii at all. Thus, the main contribution to the errors in the photometric solution clearly comes from the uncertainty in L_B/L_A, and can result in errors in k and the radii up to 4σ.

Table 10. Mean elements for CPD −59°2628

i	$80\overset{\circ}{.}58 \pm 0\overset{\circ}{.}50$	M_B/M_A	0.83 ± 0.08
ω	180°(assumed)	e	0.0 (assumed)
r_A mean	0.330 ± 0.002	r_B mean	0.273 ± 0.002
$T_{\rm eff,A}$	$32\,000 \pm 500$ K	$T_{\rm eff,B}$	$30\,000 \pm 800$ K
L_B/L_A	0.564 (y)	0.564 (b)	0.559 (v)	0.531 (u)

Then the stellar dimensions (i, radii and potentials) are fixed to their mean values from Table 8 while $T_{\rm eff,B}$ and L_A are adjusted in order to get L_B/L_A for each of the four bands. For *uvby* solutions based on the same system geometry, this allows individual *uvby* indices to be calculated from the observed combined indices.

The corresponding set of solutions is given in Table 9. Both sets of solutions agree well: temperatures and luminosities are the same, only the luminosity ratio is slightly increased, mostly for the b and u bands. Theoretical flux ratios based on NLTE atmosphere models for temperatures of 30 000 and 27 000 K only predict 0.01 higher luminosity ratio in the y–band than in v, while for the u–band, a larger change is expected but with negative sign. This is also what is seen in Table 9 where $L_B/L_A(bvy)$ have similar values and $L_B/L_A(u)$ is significantly smaller. The temperature of the secondary component is about 1000 K lower than the temperature found from the spectroscopy, but both temperatures agree within their errors.

5. Absolute dimensions and evolutionary status

From the combined standard indices in Table 1 and the luminosity ratios in Table 10, we get the individual standard indices in Table 11 using the excess and extinction values $E(b-y) = 0\overset{\rm m}{.}306$, $A_V = 1\overset{\rm m}{.}314$ from Kaltcheva & Georgiev (1993) and Crawford (1975). The calibration by Flower (1996) was adopted for the bolometric corrections.

Table 11. Astrophysical data for CPD −59°2628. $M_{\mathrm{bol},\odot} = 4.7$ is assumed, while $M_\odot = 1.989\,10^{30}$ kg and $G = 6.67259\,10^{-11}\,\mathrm{m^3\,kg^{-1}\,s^{-2}}$ are from Seidelmann (1992). K_A and K_B are taken from Col. 4 in Table 5. See text for comparison with parameters calculated for the K_A and K_B from SN

	Star A	Star B
Absolute dimensions:		
$M/M_\odot$	14.0 ± 2.0	11.7 ± 1.8
$R/R_\odot$	5.29 ± 0.25	4.38 ± 0.25
$\log g$ (cgs)	4.138 ± 0.074	4.224 ± 0.082
$v_{\mathrm{sync}} \sin i$ (km s^{-1})	180 ± 9	149 ± 8
Photometric data:		
V	10.101	10.719
$(b-y)$	0.183	0.183
m_1	−0.022	−0.011
c_1	−0.064	−0.024
$E(b-y)$	0.307	0.303
A_V	1.321	1.304
V_0	8.780	9.415
$(b-y)_0$	−0.124	−0.120
m_0	0.070	0.080
c_0	−0.125	−0.085
$[m_1]$	0.033	0.044
$[c_1]$	−0.101	−0.061
$[u-b]$	−0.035	−0.085
$\log T_{\mathrm{eff}}$	4.505 ± 0.007	4.477 ± 0.012
$\log\ L/L_\odot$	4.42 ± 0.05	4.14 ± 0.07
M_{bol}	-6.31 ± 0.12	-5.62 ± 0.17
$B.C.$	−3.07	−2.87
M_V	-3.24 ± 0.12	-2.75 ± 0.17
$(L_B/L_A)_{\mathrm{bol}}$	0.64 ± 0.19	
Distance (pc)	2600 ± 120	

The resulting absolute dimensions are given in Table 11. Andersen et al. (1980) discussed consistency between photometric and spectroscopic data when deriving absolute dimensions. Following their guidelines for a consistency check on the solutions, we note that q has been fixed by the spectroscopic analysis throughout the photometric analysis, that the luminosity ratios from the photometry and the line measurements both agree, and that rotational velocities $v \sin i$ all agree with: i) the period and radii (Table 11); ii) the NLTE analysis of the s9–s10 spectra (Sect. 3.5); iii) linewidths of rotational standards. The latter supports our assumption of synchronous rotation. We adopted the temperatures determined from the s9–s10 spectra, which agree with the ratio of temperatures from photometry. The derived data in Table 11 are thus consistent for spectroscopy and photometry. The masses have large uncertainties and the actual errors may even exceed those derived in the SBOP solution (Table 5), because of the aforementioned systematic errors from line measurements. SN do not publish any information on lines used in their investigation, so we can only note that they in fact get higher masses than we find with the data from LM.

5.1. Theoretical models, age

In Fig. 9, we have compared the two components of CPD −59°2628 with evolutionary stellar models from Claret (1995) for the chemical composition ($X = 0.70$, $Z = 0.02$). The high uncertainties in the surface gravity and effective temperatures, give large error bars in the figure. The evolutionary model tracks predict higher masses than found from the spectroscopy (see the SBOP solution in Table 5): $17 \pm 1\ M_\odot$ (A) and $15 \pm 1\ M_\odot$, but the differences are inside the shared uncertainties. Higher model masses could be caused by dependencies on model composition, but a large range of other X and Z compositions also gave high masses. Likewise, reducing the stellar components' temperatures does not lower the model masses sufficiently. The systematic errors from using HI and diffuse HeI lines for radial velocity measurements, mentioned in Sect. 3.4, are known to give 10–40% too small masses for OB–stars due to line blending (Andersen et al. 1980; Andersen 1991 and references therein). We therefore suspect that the spectroscopy underestimates the masses. Lower masses give smaller maximum velocities K_A and K_B, so as an experiment we set the K_A and K_B values 5% too small and adjusted the SBOP parameters accordingly. The resulting masses (16.3 $M_\odot$ and 13.5 $M_\odot$, star A and B respectively) agreed with model masses for the composition ($X = 0.70$, $Z = 0.02$) to within 10% – approximately the estimated error of the model masses. These model masses agree well with the masses found by SN (Table 5). It is our impression that the best fit is provided by a model with Z lower than 0.02, possibly 0.015.

In the same Fig. 9, isochrones are plotted for $\log age =$ 6.3, 6.6 and 6.8 yr by using linear interpolation in the tables by Claret (1995). The models do fit the components with respect to mass, surface gravity and temperature for ages between the $\log age = 0.0$ and 6.3 isochrones, but with substantial error bars. By assuming the same age for both components, the error bars overlap for a young age of 1.5 ± 1.0 Myr. A model with the composition ($X = 0.75$, $Z = 0.03$) gave higher masses of 18.5 and 15.5 $M_\odot$ but 1.5 Myr younger ages, which for assumed identical ages indicate a very low age of 0.2 ± 1.0 Myr. The chemically enriched field, which is rich in OB stars, favors the model with composition ($X = 0.70$, $Z = 0.02$).

For comparison, we calculated absolute parameters by using the K_A and K_B values from SN. We used our photometric values for the other parameters, i.e. k, q and i. The corresponding masses are $16.9 \pm 1.0\ M_\odot$ (A) and $14.4 \pm 0.9\ M_\odot$ (B) giving the ratio $q = 0.85 \pm 0.03$, which is reasonably close to the ratio assumed in the photometry for this purpose. Note that the errors on K_A and K_B given by SN, correspond to half the size of the errors they give for the masses – their maximum projected velocity errors may be optimistic. Resulting values of surface gravity and radius are: $\log g = 4.16 \pm 0.03$ (A) and 4.26 ± 0.04 (B), and $R_A = 5.6 \pm 0.1\ R_\odot$ and $R_B = 4.7 \pm 0.2\ R_\odot$, which in Fig. 9 gives ∼0.5 Myr lower ages than from the LM spectroscopy. But the scatter around a common isochrone is

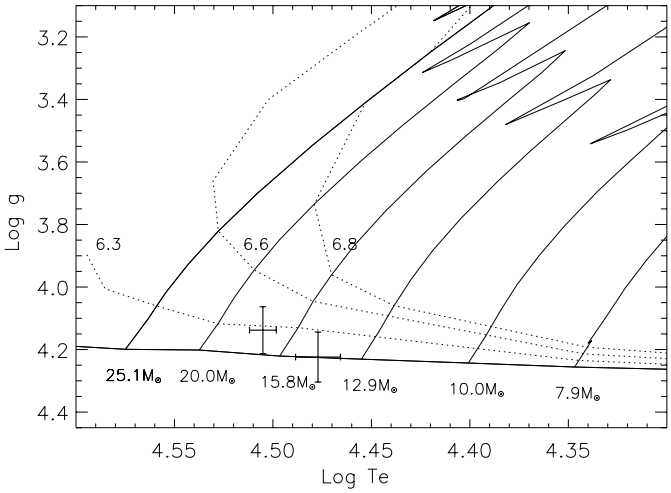

Fig. 9. Evolutionary diagram for $\log g$ versus $\log T_{\rm eff}$ from Claret (1995) and the CPD −59°2628 A and B components. Error bars are included from Table 11. Dotted lines are isochrones with $\log age$ indicated while the solid lines are evolutionary tracks for different masses

large when considering the small errors. Rotational velocities are $V_{{\rm sync},A} = 192\pm4$ and $V_{{\rm sync},B} = 159 \pm 6$. The resulting photometric parameters are: luminosities $\log L_A = 4.477 \pm 0.034$ and $\log L_B = 4.199 \pm 0.057$, which gives the ratio $L_B/L_A = 0.64 \pm 0.15$, and the magnitudes $M_{{\rm bol},A} = -6.452 \pm 0.084$, $M_{{\rm bol},B} = -5.758 \pm 0.143$, $M_V, A = -3.382 \pm 0.084$ and $M_V, B = -2.888 \pm 0.143$, giving the distance modulus $(m - M) = 12.22 \pm 0.08$.

5.2. Cluster membership

The absolute dimensions and bolometric magnitude from Table 11 yield a distance to the binary of $d = 2.60 \pm 0.12$ kpc or a true distance modulus of $(m - M) = 12.07 \pm 0.10$. Massey et al. (1993) determined a true distance modulus for the cluster of 12.49 ± 0.09 based on photometry of 37 massive stars in the cluster, while Kaltcheva & Georgiev (1993) reach 11.54 ± 0.64 by using $uvby - \beta$ photometry of 26 stars. Thus, our distance agrees more with that of Kaltcheva & Georgiev, but the differences may be because the cluster is extended along the line of sight. From our spectroscopic analysis, we find a systemic velocity of -19 ± 9 km s^{-1}. With 25 stars in Trumpler 16, including CPD −59°2628 and other binaries, LM derive a mean heliocentric radial velocity for Trumpler 16 of -23 ± 1.5 km s^{-1}. CPD −59°2628 is therefore, we believe, a member of Trumpler 16 as found by Kaltcheva & Georgiev (1993) and LM. SN find a systemic velocity for the binary of -5 ± 4 km s^{-1}, a value that deviates from the cluster velocity. A third body could explain a seemingly variable systemic velocity, but neither our analysis of the spectra s1–s10, spanning almost 10 years in time, nor the WD–solutions (Sect. 4.3) indicate that this is the case.

6. Conclusions

We have used high–precision photometry together with reanalysed spectrographic data in our analysis of CPD −59°2628 to determine physical parameters of the components. New high–resolution spectra were used for an independent check on the new orbital period and photometric solution. The system is well–detached, consists of two similar stars with spectral types O9.5 V and B0 V having ages below 3 Myr. Temperatures of the components seem to be 1000 K higher when determined from our spectroscopic analysis, than from the photometry.

Evolutionary models predict slightly higher masses than found with the spectroscopy from LM, in agreement with the orbital parameters derived by SN. We explain the lower masses with the poorness of the available spectroscopic data from LM and systematic errors in their line measurements. Our orbital solution agrees with the one from SN within shared errors, except from minor differences between phases for the ephemeris, and between the systemic velocities. CPD −59°2628 resembles the early–B binary V578 Mon (Hensberge et al. 2000), both with regard to dimensions and spectral types of the components.

We determine a distance to CPD −59°2628 from the derived physical parameters of the components, that together with the systemic velocity confirms its membership in Trumpler 16. The systemic velocity disagrees slightly with the one by SN.

There is an urgent need for new high–resolution spectroscopic data of the system in order to obtain precise masses by application of spectral component disentangling.

Acknowledgements. We thank Herman Hensberge, ROB, for providing rotationally broadened NLTE model lines and acknowledge him for discussions and advice during the spectroscopic analysis. We gratefully acknowledge Michael I. Andersen for his assistance in the reanalysis of the radial velocity data and S. A. Naftilan for a careful reading of the paper. LMF is grateful to Nordic Optical Telescope[1] where a part of this work was made during a stay under a studentship. Part of this research was carried out in the framework of the projects "IUAP P4/05" financed by the Belgian DWTC/SSTC, and "Structure and evolution of stars - new insight from eclipsing binaries and pulsating stars" carried out at Aarhus University and Copenhagen University and supported by The Danish National Science Research Council. This work has been supported by the Belgian Fund for Scientific Research (FWO) and has made use of the Simbad database, operated by the CDS, Strasbourg, France. We have used the `ESO-MIDAS` software, the `NOAO-IRAF/DAOPHOT` package, and the `SBOP` and Wilson–Devinney programmes.

[1] Nordic Optical Telescope is operated on the island of La Palma jointly by Denmark, Finland, Iceland, Norway, and Sweden, in the Spanish Observatorio del Roque de los Muchachos of the Instituto de Astrofisíca de Canarias.

References

Andersen, J. 1991, A&AR, 3, 91

Andersen, J., Clausen, J. V., & Nordström, B. 1980, in Close Binary Stars: Observations and Interpretation, IAU Symposium No. 88, ed. M. J. Plavec, D. M. Popper, & R. K. Ulrich, 81

Butler, K. 1994, Manual (STScI Mirror Site), `http://icarus.stsci.edu/~hulbert/ccp7/Docs/detail.ps`

Böhm–Vitense, E. 1981, ARA&A, 19, 295

Catanzaro, G. 1997, Ap&SS, 257, 161

Claret, A. 1995, A&AS, 109, 441

Crawford, D. L. 1975, PASP, 87, 481

Diaz-Cordoves, J., Claret, A., & Gimenez, A. 1995, A&AS, 110, 329

Etzel, P. B. 1985, SBOP – Spectroscopic Binary Orbit Program, Program's Manual

FitzGerald, M. P. 1970, A&A, 4, 234

Flower, P. J. 1996, ApJ, 469, 355

Giddings, J. 1981, Ph.D. Thesis, University of London

Gray, D. F. 1976, The Observation and Analysis of Stellar Photospheres (J. Wiley & Sons)

Hensberge, H., Pavlovski, K., & Verschueren, W. 2000, A&A, 358, 553

Jenniskens, P., & Désert, X. 1994, A&AS, 106, 39

Kaltcheva, N. T., & Georgiev, L. N. 1993, MNRAS, 261, 847

Kaufer, A., Stahl, O., & Tubbesing, S., et al. 1999, The ESO Messenger, 95, 8

Kurucz, R. L. 1979, ApJS, 40, 1

Kurucz, R. L. 1992, Rev. Mex. Astron. Astrofis., 23, 45

Kwee, K. K., & van Woerden, H. 1956, Bull. Astron. Neth., 12, 323

Lehmann–Filhes, R. 1894, AN, 163, 17

Levato, H., & Malaroda, S. 1982, PASP, 94, 807

Levato, H., Malaroda, S., Morrell, N., et al. 1991 (LM), ApJS, 75, 869

Massey, P., & Johnson, J. 1993, AJ, 105, 980

Nordlund, Å., & Vaz, L. P. R. 1990, A&A, 228, 231

Ogura, K., & Ishida, K. 1981, PASJ, 33, 149

Popper, D. M., 1980, ARA&A, 18, 115

Seidelmann, K. 1992, Explanatory Supplement to the Astronomical Almanac, ed. K. Seidelmann

Slettebak, A., Collins, G. W., Boyce, P. B., et al. 1975, ApJS, 29, 137

Solivella, G. R., & Niemela, V. S. 1999 (SN), Rev. Mex. Astron. Astrofis., 8, 145

Stahl, O., Kaufer, A., & Tubbesing, S. 1999, The FEROS spectrograph, in Optical and Infrared Spectroscopy of Circumstellar Matter, ed. E. Guenther, B. Stecklum, & S. Klose, ASP Conf. Ser., 188, 331

Sterken, C. 1983, The ESO Messenger, 33, 10

Sterken, C. 1994, in The Impact of Long-Term Monitoring on Variable-Star Research, NATO ARW, ed. C. Sterken, & M. de Groot, NATO ASI Series C, 436 (Kluwer Ac. Publ.), 1

Sterken, C., Freyhammer, L., Arentoft, T., & van Genderen, A. M. 1999, A&A, 346, L33

Stetson, P. 1987, PASP, 99, 191

Tuairisg, S. Ó., Cami, J., Foing, B. H., et al. 2000, A&AS 142, 225

van Hamme, W. 1993, AJ, 106, 2096

Vaz, L. P. R. 1986, Rev. Mex. Astron. Astrofis., 12, 199

Vaz, L. P. R., & Nordlund, Å. 1985, A&A, 147, 281

Vaz, L. P. R., Andersen, J., & Rabello Soares, M. C. A. 1995, A&A, 301, 693

Vaz, L. P. R., Cunha, N. C. S., Vieira, E. F., & Myrrha, M. L. M. 1997, A&A, 327 1094

Vrancken, M., Hensberge, H., David, M., et al. 1997, A&A, 320, 878

Walborn, N. R. 1982, AJ, 87, 1300

Walborn, N. R., & Fitzpatrick, E. L. 1990, PASP, 102, 379

Wilson, R. E. 1993, in New Frontiers in Interacting Binary Star Research, ed. K. C. Leung, & I.-S. Nha, ASP Conf. Ser., 38, 91

Wilson, R. E., & Devinney, E. J. 1971, ApJ, 182, 539

Wood, D. B. 1971, AJ, 76, 701